Preprints of the 21st IFAC World Congress (Virtual)
Berlin, Germany, July 12-17, 2020

High Precision Positioning Using Acceleration and Displacement Sensors in Piezo-driven Stage Systems

Kenta Seki * **Makoto Iwasaki** *

* *Department of Electrical and Mechanical Engineering, Nagoya Institute of Technology, Gokiso, Showa, Nagoya, Aichi, 4668555 Japan (e-mail: k-seki@nitech.ac.jp).*

Abstract: This paper presents a control design approach to compensate for the phase delay and resonant vibration in the piezo-driven stage systems. A target piezo-driven stage is installed in a capacitive sensor to detect the accurate stage displacement, however, the sensing system generally includes a phase delay due to the data conversion process and lowpass filters in the amplifier to remove the sensor noise. In this study, a MEMS acceleration sensor signal is integrated into the displacement signal detected by a capacitive sensor to improve the phase characteristics at a high frequency range, and the composite filters are designed to synthesize two sensor signals. In addition, the acceleration minor-loop is added to robustly suppress the resonant vibration against the frequency variations. The effectiveness of the design approach is verified by conducting experiments using a commercial piezo-driven stage system.

Keywords: piezo actuator, composite filter, acceleration sensor, vibration suppression

1. INTRODUCTION

Piezoelectric actuator is an actuator using inverse piezoelectric effect. Due to the advantages such as high positioning resolution and power density, these actuators are universally used in micro/nano positioning applications (Devasia et al. 2007)(Fleming and Leang 2014). However, the positioning accuracy deteriorates owing to the nonlinearities such as hysteresis and creep (Goldfarb and Celanovic 1997). Hysteresis leads to poor repeatability, while creep severely deteriorates the low-frequency and static positioning accuracy. Another deterioration factor is the presence of the low-damping mechanical resonances. These dynamics leads to residual vibration when a high-frequency component is present in the voltage applied to the actuator.

To enhance the positioning accuracy, these nonlinearities and mechanical resonances must be compensated. Feedback control with integral action that employs high-resolution position sensors is a common approach, where a high-gain controller effectively reduces the nonlinearities. As the control bandwidth is limited by the presence of mechanical vibration modes, the damping control approaches have been proposed: notch filter (Leang and Devasia 2007), integral resonance control (Fleming et al. 2010), and self-sensing technique using a bridge circuit (Seki and Iwasaki 2015). Although these approaches are effective for suppressing the vibration, it is difficult to sufficiently expand the control bandwidth considering the frequency variations. In addition, the sensing system causes a phase delay owing to the detection circuit and filter used to reduce the sensor noise, resulting in a decrease in the phase margin of the system. As a solution to overcome the robust vibration suppression and phase delay, multi-sensing systems which expand the conventional single-input single-output (SISO) systems have been proposed to find a breakthrough in the conventional control performances. For examples, a strain sensor or load-side position sensor is integrated into the position control system based on the motor position sensor to expand the control bandwidth by suppressing the mechanical resonant vibrations in industrial machineries (Seki et al. 2009) (Sakata et al. 2014).

This study presents a design approach of integrating an acceleration sensor with a displacement sensor to achieve the expansion of the control bandwidth and robust vibration-suppression performance against frequency variations simultaneously. The target piezo-driven stage system is installed in the capacitive sensor to detect the accurate stage displacement. However, the sensing system includes the phase delay owing to the data conversion process and the lowpass filters in the amplifier. Low-cost MEMS acceleration sensors are widely employed in the mechatronic systems (Antonello and Oboe 2012). In this study, the signal detected by the MEMS acceleration sensor is integrated into the displacement signal to recover the phase delay, whereas the composite filters (Stoten 2001) are designed to integrate the two sensing signals without mutual interference. This approach can be implemented at a low computational cost because the composite filters are simple structures. In addition, the acceleration sensor can directly detect the mechanical vibration signal. Thus, the resonant vibration can be suppressed by adding an equivalent velocity feedback based on the acceleration signal. The effectiveness of the design approach is verified by conducting experiments using the commercial piezo-driven stage system.

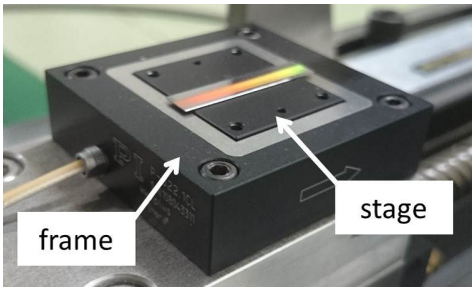

Fig. 1. Overview of positioning stage system.

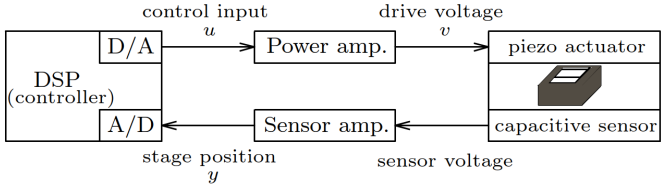

Fig. 2. System configuration of the positioning stage system.

2. POSITIONING SYSTEM USING PIEZOELECTRIC ACTUATOR

2.1 System configuration

Figure 1 shows an overview of the positioning stage system driven by a stacked piezoelectric actuator (P-622.1, Physik Instrumente GmbH & Co. KG.). The stage is supported in a single direction by the flexure hinge, where the displacement of the piezoelectric actuator is amplified by the hinge mechanism. The stage position is measured by a capacitive sensor installed in the stage system.

Figure 2 shows the system configuration. The sensor voltage is amplified by a sensor amplifier (E-610, Physik Instrumente GmbH & Co. KG.). The stage position y is transferred to a controller board (DS1103, dSPACE GmbH) with a sampling period of 0.1 [ms]. The piezoelectric actuator is driven based on the control input u generated by the controller through a power amplifier (HSA 4014, NF Corporation).

2.2 Plant dynamics

Solid lines in Fig. 3 show the frequency characteristic of the stage position y for the control input u, where the characteristics are measured by a swept-sine excitation test using a frequency response analyzer (FRA5097, NF Corporation). The figure shows that the mechanism includes mechanical resonances owing to the elastic hinges at 340 [Hz] and 560 [Hz]. In addition, the phase delay appears above 10 [Hz]. Based on Fig. 3, the linear dynamics can be expressed as a mathematical model $P_c(s)$, consisting of the resonant vibration modes and a dead time component:

$$P_c(s) = \frac{y}{u} = K_g \left(\sum_{i=1}^{2} \frac{k_{pi}}{s^2 + 2\zeta_{pi}\omega_{pi}s + \omega_{pi}^2} \right) \frac{\omega_l}{s + \omega_l} e^{-Ls}, \quad (1)$$

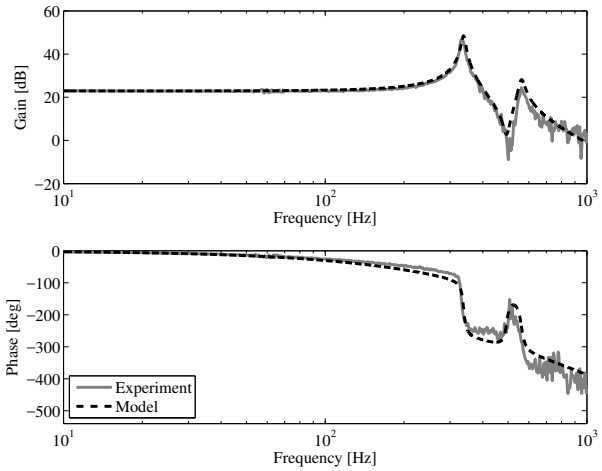

Fig. 3. Plant characteristics.

Table 1. Parameters of plant model.

ω_{p1}[rad/s]	$2\pi \times 340$	ζ_{p1}	0.016	k_{p1}	2.5
ω_{p2}[rad/s]	$2\pi \times 560$	ζ_{p2}	0.025	k_{p2}	1.3
ω_l [rad/s]	$2\pi \times 382$	L [s]	4.0×10^{-4}	K_g	2.0×10^7

where K_g is constant gain including the power and sensor amplifiers, ω_{pi} is natural angular frequency of ith vibration mode, ζ_{pi} is damping coefficient of ith vibration mode, k_{pi} is modal constant of ith vibration mode, ω_l is cut-off frequency of lowpass filter in the sensor amplifier, and L is equivalent dead time. The dead time is caused by the capacitive sensor and the sensor amplifier because the cut-off frequency of the power amplifier is over 10 [kHz]. Broken lines in Fig. 3 show the frequency characteristic of the mathematical model $P_c(s)$, while Table 1 lists identified parameters of the model.

2.3 SISO control system

Figure 4 shows the block diagram of a traditional SISO feedback control system based on the displacement signal, where the feedback compensator $C_n(s)$ generally includes notch filter and proportional-integral (PI) compensator. The transfer function of $C_n(s)$ is as follows.

$$C_n(s) = \left(K_P + \frac{K_I}{s} \right) \cdot \prod_{i=1}^{2} \frac{s^2 + 2\zeta_{ni}\omega_{ni}s + \omega_{ni}^2}{s^2 + 2\zeta_{di}\omega_{ni}s + \omega_{ni}^2} \quad (2)$$

The notch filter is designed to reduce the gain peaks of the mechanical vibration modes. The gains of the PI compensator are tuned to accommodate the stability, transient response, and control bandwidth. Table 2 lists the parameters of $C_n(s)$. Figure 5 shows the closed-loop characteristics, where the solid lines indicate the nominal condition without resonant frequency variations, dotted and broken lines indicate the characteristics under the frequency variations $\pm$ 70 [Hz]. This figure shows that the notch filter cannot obtain robust vibration-suppression performance against frequency variations. In addition, the phase delay needs to be improved to expand the control bandwidth.

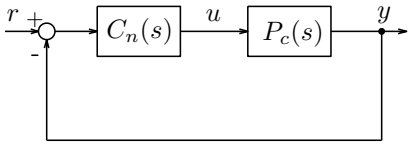

Fig. 4. SISO feedback control system.

Table 2. Parameters of $C_n(s)$.

K_P	0.014	K_I	7.58		
ω_{n1}[rad/s]	$2\pi \times 340$	ζ_{n1}	0.016	ζ_{d1}	1.0
ω_{n2}[rad/s]	$2\pi \times 560$	ζ_{n2}	0.025	ζ_{d2}	1.0

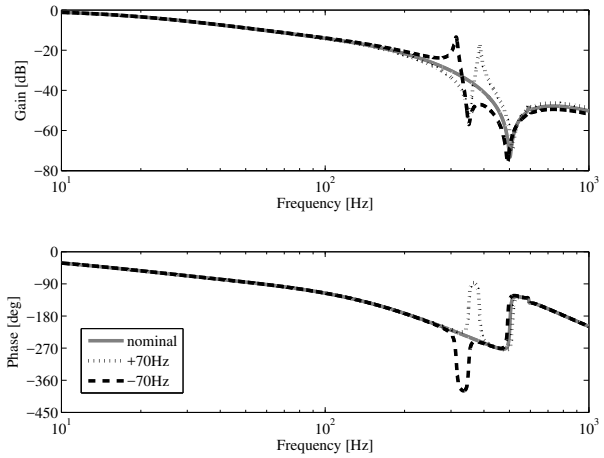

Fig. 5. Closed-loop characteristics of SISO feedback control system with notch filter

3. CONTROLLER DESIGN COMBINED WITH ACCELERATION SIGNAL

3.1 Frequency characteristic of acceleration sensor

Figure 6 shows an overview of the positioning stage with a MEMS acceleration sensor (ADXL-335, Analog Devices, Corp.), where the sensor is attached to the table for a basic examination. The acceleration signal is transferred in the controller through the A/D converter. Solid lines in Fig. 7 show the frequency characteristic of the acceleration signal y_a for the control input u. Based on these characteristics, the linear dynamics $P_a(s)$ can be modeled as:

$$P_a(s) = \frac{y_a}{u} = K_{gs}s^2\left(\sum_{i=1}^{2}\frac{k_{pi}s^2}{s^2+2\zeta_{pi}\omega_{pi}s+\omega_{pi}^2}\right)e^{-L_a s}, \quad (3)$$

where $K_{ga} = 1.1\times10^7$: plant and sensor gain and $L_a = 2\times10^{-4}$: equivalent dead time of the acceleration sensor. The parameters of the vibration modes are the same as Table 1. Broken lines in Fig. 7 show the frequency characteristics of the mathematical model $P_a(s)$.

3.2 Control structure

Figure 8 shows the block diagram of proposed control system using the displacement and acceleration sensors,

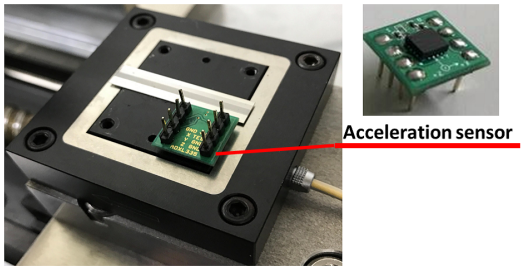

Fig. 6. Overview of positioning stage system with acceleration sensor.

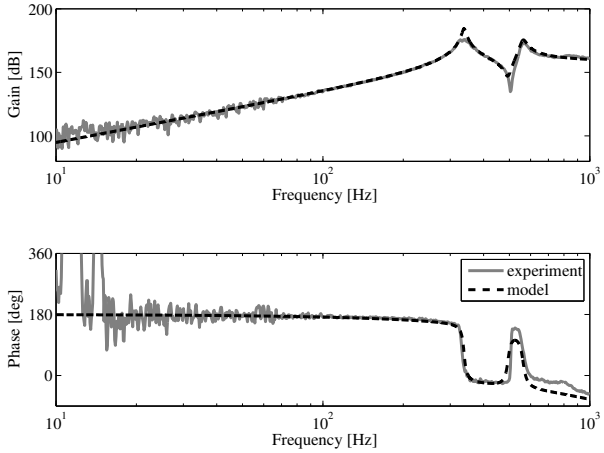

Fig. 7. Frequency characteristics of the acceleration signal for control input.

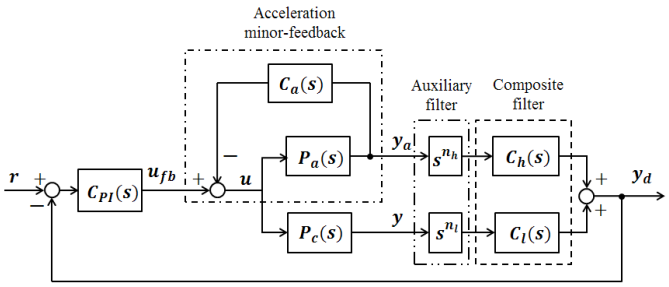

Fig. 8. Block diagram of control system combined with the acceleration sensor.

where r: displacement reference, $C_{PI}(s)$: feedback compensator, u_{fb}: output of feedback compensator, $C_a(s)$: acceleration minor-loop compensator, $C_l(s)$ and $C_h(s)$: composite filters, s^{n_h} and s^{n_l}: auxiliary filters, y_d: composite displacement signal. In the composite filters part, the displacement signal with small phase delay is generated by fusing the signals of the displacement and acceleration sensors. A minor loop that feeds back the signal detected by the acceleration sensor is designed to attenuate the gain peak at the resonant frequencies in the plant.

Design of composite filters To recover the phase delay shown in Fig. 3, the signal from the acceleration sensor y_a is integrated into the displacement signal y using the composite filters. The auxiliary filter for the acceleration signal is designed as a double integrator because the

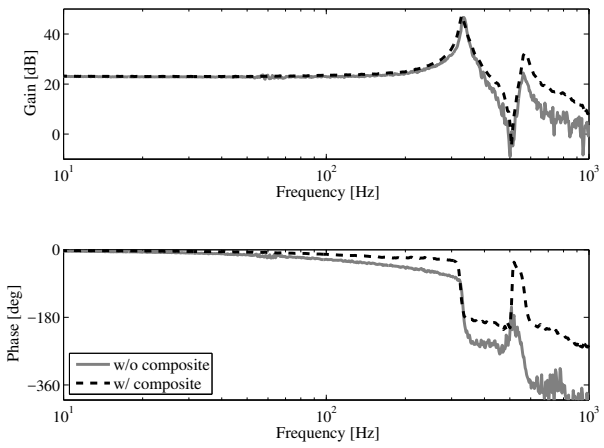

Fig. 9. Frequency characteristics of plant with and without the composite filter.

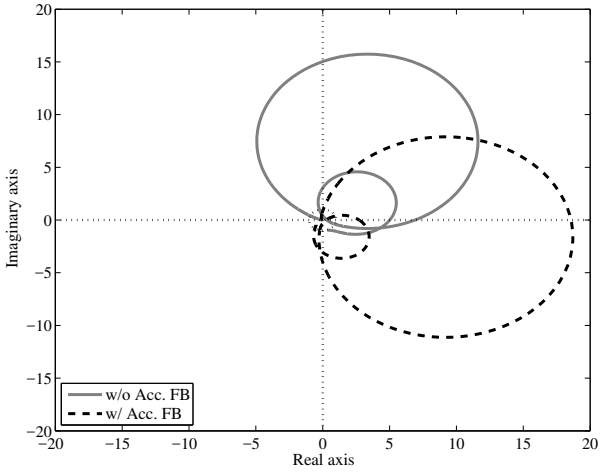

Fig. 10. Vector loci of acceleration minor-loop.

dimension of the output signal is displaced. Thus, the power indices of each auxiliary filter are set as $n_h = -2$ and $n_l = 0$ (Stoten 2001). To ensure the unity gain and non-phase delay in the composite filters, the following condition should be satisfied.

$$C_l(s) + C_h(s) = 1 \tag{4}$$

The filter $C_l(s)$ for the displacement signal is designed as a lowpass filter to reduce the noise at high frequency region, while the filter $C_h(s)$ for the acceleration signal is designed as a highpass filter to prevent the drift owing to the signal bias and integral action of the auxiliary filter. Based on the design guideline, each filter is designed as follows:

$$C_l(s) = \frac{a_2 s^2 + a_1 s + a_0}{s^3 + a_2 s^2 + a_1 s + a_0}, \tag{5}$$

$$C_h(s) = \frac{s^3}{s^3 + a_2 s^2 + a_1 s + a_0}. \tag{6}$$

The filter coefficients are arbitrarily set considering the separation frequency and each sensor performance. In this study, each coefficient as Butterworth filter is defined as follows:

$$a_0 = a^3, \tag{7}$$

$$a_1 = 2a^2, \tag{8}$$

$$a_2 = 2a. \tag{9}$$

The coefficient a in (6), (7), and (8) is set as $2\pi \times 100$ [rad/s] based on the phase characteristics in Fig. 3 and the acceleration characteristics in Fig. 7.

Figure 9 shows the plant characteristics obtained by conducting the swept-sin excitation test, where the solid lines indicate the characteristic of y for u shown in Fig. 3 and broken lines indicate the characteristics of y_d for u using composite filters. Figure 9 shows that the phase delay is recovered at high frequency range.

Vibration suppression by acceleration feedback The transfer function with acceleration minor-loop in the Fig. 8 can be expressed as follows:

$$P_{ac}(s) = \frac{y_d}{u_{fb}} = \frac{1}{1 + P_a(s)C_a(s)} P_d(s), \tag{10}$$

Table 3. Parameters of $C_a(s)$.

K_a	5.0×10^{-8}	T_i	2.0×10^{-3}	ω_a [rad/s]	$2\pi \times 5.0$

where $P_d(s)$ is the characteristic of dotted lines in Fig. 9. To attenuate the gain peaks of vibration modes, the sensitivity gain of the acceleration minor-loop should be reduced at each resonant frequency. Therefore, minor-loop compensator $C_a(s)$ should be designed to draw the vector locus of $P_a(s)C_a(s)$ away from $(-1, 0)$ on the complex plane (Atsumi et al. 2007). Solid line of Fig. 10 shows vector locus of $P_a(s)$. In order to reduce the sensitivity gain of the two vibration modes, it is necessary to design the compensator $C_a(s)$ that delays the phase by 90 [deg] near the resonance frequencies. Based on the design guideline, the compensator $C_a(s)$ is designed as follows:

$$C_a(s) = \frac{K_a}{T_i s + 1} \cdot \frac{s}{s + \omega_a}, \tag{11}$$

where the lowpass filter is designed to tune the phase delay and the highpass filter is designed to eliminate bias signal. The designed parameters are listed in Table 3, while the vector locus of $P_a(s)C_a(s)$ is shown as a broken line of Fig. 10. Figure 11 (a) and (b) show the sensitivity characteristics and plant characteristics with the acceleration minor-loop of y for u_{fb}. The sensitivity gain in the Fig. 11 (a) can be reduced at resonant frequencies. As a result, the gain peaks can be attenuated by applying the compensator $C_a(s)$ as shown in Fig. 11 (b).

Design of feedback compensator Since the vibration modes are damped by the acceleration feedback, the feedback compensator $C_{PI}(s)$ is designed as a simple PI compensator as

$$C_{PI}(s) = K_P + \frac{K_I}{s}. \tag{12}$$

Each gain is designed considering the stability of the control system and the transient characteristic for the reference. Figure 12 shows the closed-loop characteristics (y_d/r) of the designed control system, where the solid lines indicate nominal condition without resonant frequency variations and dotted and broken lines indicate the characteristics with the resonant frequency variations ± 70

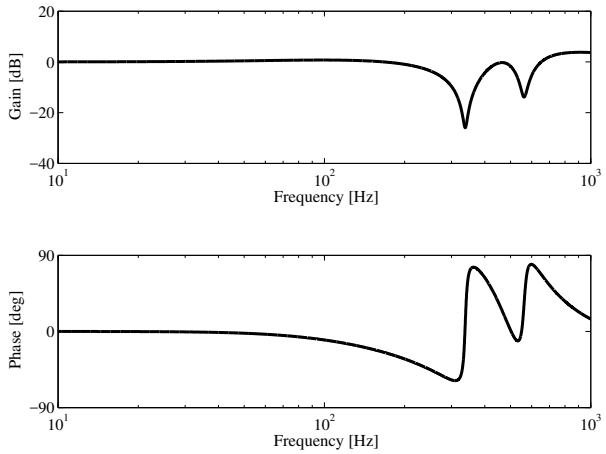

(a) Sensitivity characteristic (u/u_{fb}).

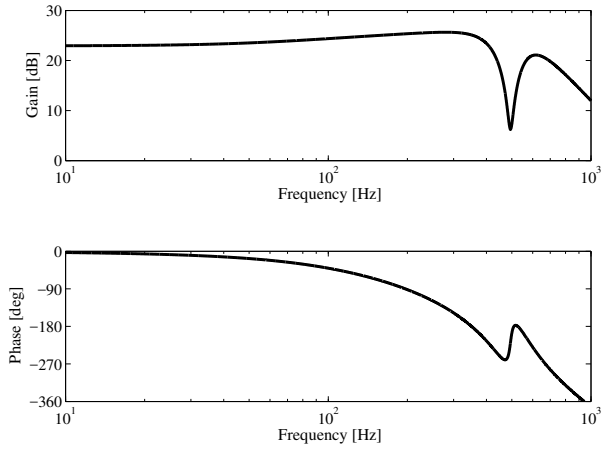

(b) Frequency characteristic (y/u_{fb}).

Fig. 11. Characteristics of the acceleration minor-loop.

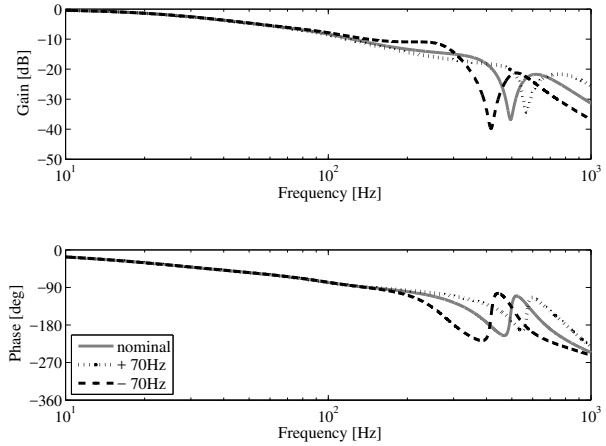

Fig. 12. Closed-loop characteristics with acceleration feedback and composite filter.

[Hz]. This figure also shows that the gain peaks can be sufficiently suppressed during frequency variations.

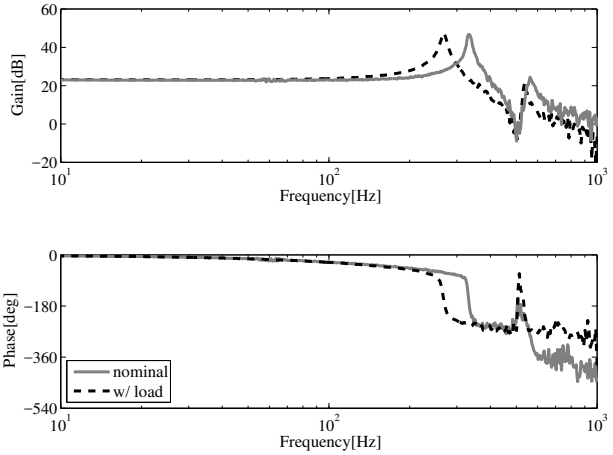

Fig. 13. Frequency characteristics of the plant with load.

4. EXPERIMENTAL VERIFICATIONS

The effectiveness of the proposed control system is verified by conducting experiments. In the experiments, resonant frequency variations are simulated by attaching a load on the stage. Figure 13 shows the frequency characteristics of the piezo-driven stage, where the solid lines indicate the nominal condition without load and the broken lines indicate the characteristics with load. This figure also shows that the resonant frequency of the 1st vibration mode fluctuates by -70 [Hz]. Figure 14 shows the error waveforms between the position reference and response $(r - y)$ under the nominal condition, while Fig. 15 shows the error waveforms under frequency variations. The upper figures of Figs. 14 and 15 show the positioning results for the reference 50 μm and the bottom ones show the positioning results for the reference 100 μm. Solid lines indicate the responses for the proposed control system and broken lines indicate the responses for the SISO feedback system with notch filter as shown in Fig. 5. To compare the effectiveness of the improvement of the phase delay, the gains of PI compensator in each control system are tuned to the same phase margin of 55 [deg]. The gain-crossover frequency of SISO control system is 17.1 [Hz], while the gain-crossover frequency of the proposed control system is 34.4 [Hz].

These results show that the position response of proposed control system is faster than the SISO system because the control bandwidth can be expanded by recovering the phase delay. In addition, the residual vibration can be sufficiently suppressed against resonance frequency variation.

5. CONCLUSIONS

This study presented a design approach using displacement and acceleration sensors for the positioning stage driven by the piezoelectric actuator. The target stage system can measure the stage displacement with high resolution using the capacitance sensor, while the phase delay increases in the high frequency region owing to the filters and signal detection circuit. To recover the phase delay, the composite filters were designed to fuse the displacement and acceleration signals. In addition, the gain peaks at the

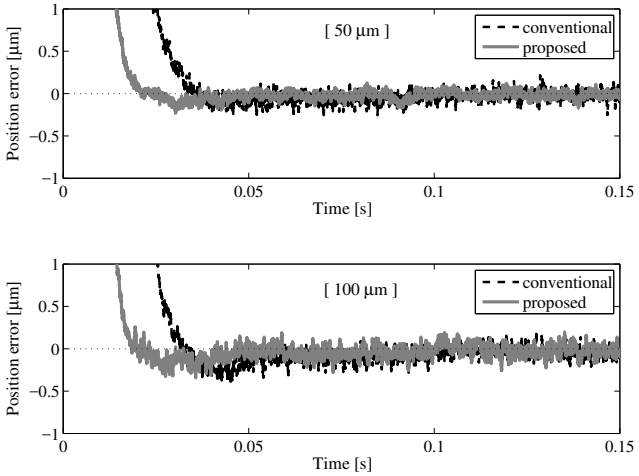

Fig. 14. Position error waveforms for the step references under nominal condition.

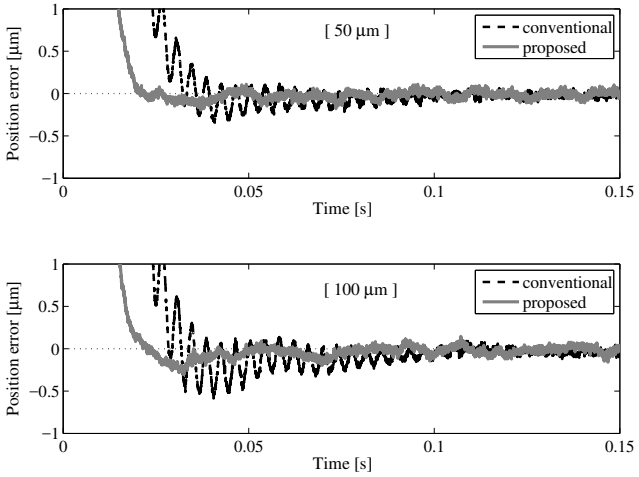

Fig. 15. Position error waveforms for the step references under resonant frequency variations.

resonance frequencies were reduced by designing a minor-loop based on the acceleration signal. Robust vibration suppression performance against the resonance frequency variations can thus be achieved, because the resonant vibration can be directly detected by the sensor. The effectiveness of the designed control system was verified by conducting experiments using the piezo-driven stage system.

REFERENCES

Antonello, R. and Oboe, R. (2012) Exploring the Potential of MEMS Gyroscopes: Successfully Using Sensors in Typical Industrial Motion Control Applications. *IEEE Industrial Electronics Magazine*, **6**(1), 14–24.

Atsumi, T., Okuyama, A., and Kobayashi, T. (2007) Track-Following Control Using Resonant Filter in Hard Disk Drives. *IEEE/ASME Transactions on Mechatronics*, **12**(4), 472–479.

Devasia, S., Eleftheriou, E., and Moheimani, S. O. R. (2007) A Survey of Control Issues in Nanopositioning. *IEEE Transactions on Control Systems Technology*, **15**(5), 802–823.

Fleming, A. J., Aphale, S. S., and Moheimani, S. O. R. (2010) A New Method for Robust Damping and Tracking Control of Scanning Probe Microscope Positioning Stages. *IEEE Transactions on Nanotechnology*, **9**(4), 438–448.

Fleming, A. J. and Leang, K. K. (2014) Design, Modeling and Control of Nanopositioning Systems. *Springer*.

Goldfarb, M. and Celanovic, N. (1997) A Lumped Parameter Electromechanical Model for Describing the Nonlinear Behavior of Piezoelectric Actuators. *Journal of Dynamic Systems, Measurement, and Control*, **119**(3), 478–485.

Leang, K. K. and Devasia, S. (2007) Feedback-Linearized Inverse Feedforward for Creep, Hysteresis, and Vibration Compensation in AFM Piezoactuators. *IEEE Transactions on Control Systems Technology*, **15**(5), 927–935.

Sakata, K., Asaumi, H., Hirachi, K., Saiki, K., and Fujimoto, H. (2014) Self Resonance Cancellation Techniques for a Two-Mass System and Its Application to a Large-Scale Stage. *IEEJ Journal of Industry Applications*, **3**(6), 455–462.

Seki, K., Mochizuki, K., Iwasaki, M., and Hirai, H. (2009) High-Precision Positioning Considering Suppression of Resonant Vibration Modes by Strain Feedback. *Proc. of the 35th Annual Conference of the IEEE Industrial Electronics Society*, 3114–3119.

Seki, K. and Iwasaki, M. (2015) Application of Self-sensing Technique for Position Control Considering Vibration Suppression in Piezo-driven Stage. *IEEE International Conference on Mechatronics*, 274–279.

Stoten, D. P. (2001) Fusion of kinetic data using composite filters. *Proc. of the Institution of Mechanical Engineers, Part I: Journal of Systems and Control Engineering*, **215**(5), 483–497.